Clinical Neurophysiology 122 (2011) 1505–1517

Contents lists available at ScienceDirect

Clinical Neurophysiology

journal homepage: www.elsevier.com/locate/clinph

Age trends and sex differences of alpha rhythms including split alpha peaks

A.K.I. Chiang [a,b,*], C.J. Rennie [a,b,c], P.A. Robinson [a,b], S.J. van Albada [a,b,d], C.C. Kerr [a,b,e]

[a] School of Physics, University of Sydney, NSW 2006, Australia
[b] Brain Dynamics Centre, Westmead Millennium Institute, Sydney Medical School – Western, University of Sydney, Westmead, Australia
[c] Department of Medical Physics, Westmead Hospital, Westmead, NSW 2145, Australia
[d] Institute of Neuroscience and Medicine – Neuromodulation INM-7, Research Center Jülich, Leo-Brandt-Straße, D-52425 Jülich, Germany
[e] Neurosimulation Laboratory, Downstate Medical Center, State University of New York, Brooklyn, NY 11203, USA

ARTICLE INFO

Article history:
Accepted 18 January 2011
Available online 23 February 2011

Keywords:
Development
Aging
EEG
Alpha rhythm
Split alpha
Double alpha

HIGHLIGHTS

- Single and double alpha peaks characterized in a sample of 1498 subjects.
- Systematic age trends found in alpha frequency, position, and power.
- Results are consistent with all subjects having posterior and frontal alpha, often with distinguishable frequencies.

ABSTRACT

Objective: To investigate age trends, sex differences, and splitting of alpha peaks of the EEG spectrum in the healthy population.
Methods: An automated multi-site algorithm was used to parametrize the alpha rhythm in 1498 healthy subjects aged 6–86 years. Alpha peaks identified from multiple electrode sites were organized into clusters of similar frequencies whose sex differences and age trends were investigated.
Results: Significant age-related trends were observed for frequency, position, and amplitude of dominant alpha peaks. Occipital sites had alpha clusters of higher average frequency, higher power, and greater presence across the scalp. Frequency and power differences were found between the sexes.
Conclusion: Observed increases in alpha frequency in children and decreases in the elderly were consistent with those from earlier studies. A large fraction of participants (≈44%) showed multiple distinct alpha rhythm thus investigations which only examine the alpha frequency with the highest peak power can produce misleading results. The strong dependence of alpha frequency on age and anterior–posterior position indicates use of a fixed alpha frequency band is insufficient to capture the full characteristics of the alpha rhythm.
Significance: This study establishes alpha rhythm parameter ranges (including power and frequency) in the healthy population, and quantifies the variation in alpha frequency across the scalp. The automated characterization enables objective evaluations of alpha band activities over large samples. These findings are potentially useful in testing theories of alpha generation, where splitting of the alpha rhythm has been theoretically predicted to occur in individuals with large differences in axon length between anterior and posterior corticothalamic loops.

1. Introduction

The alpha rhythm is the most prominent feature observed in the human electroencephalogram (EEG), and is strongest when the subject is in an eyes-closed relaxed state (Niedermeyer and Lopes da Silva, 2004). It is suppressed by attention or mental effort, though this attenuation varies greatly between individuals and experimental conditions (Shaw, 2003). The normal alpha rhythm varies in amplitude from one individual to another, and a small minority of people with normal brain function do not show an alpha rhythm (Niedermeyer and Lopes da Silva, 2004). An alpha-free low voltage EEG may also develop in adult life in certain clinical conditions such as Huntington's chorea (Scott et al., 1972). Activity is still present in the alpha band, but there is not necessarily a spectral peak, which is required for the identification of the alpha rhythm. The frequency of the alpha rhythm increases from approximately 3–5 Hz at birth until an adult value near 10 Hz is reached

* Corresponding author. Address: Physics Annexe, University of Sydney, NSW 2006, Australia. Tel.: +61 4 02950186; fax: +61 2 93517726.
E-mail address: chiang@physics.usyd.edu.au (A.K.I. Chiang).

1388-2457/$36.00
doi:10.1016/j.clinph.2011.01.040

at around 20 years of age (Marshall et al., 2002), followed by a slow decrease thereafter (Dustman et al., 1999). There are mixed reports of changes in the alpha rhythm in adulthood (Duffy et al., 1984, 2004). However, recent studies with large sample sizes have found dominant alpha frequencies to decrease with age in adults independent of pathology (Aurlien et al., 2004, 2010). Alpha rhythm is observed across the entire scalp, and there is some evidence that its frequency is anticorrelated with head size (Nunez Paul et al., 1978, 2006), though a recent MRI study by Valdés-Hernández et al. (2010) suggests it may instead be independent. A reduction of the alpha frequency can occur in demented patients or due to exogenous intoxication (e.g., with alcohol) (Samson-Dollfus et al., 1997). Alpha frequency systematically changes with cognitive impairment Bengston and Schaie, 1999.

Various peaks in the alpha band have been noted in the literature. One distinction is between frontal and occipital alpha, as determined by the location where the peak is most prominent; another is between "fast" and "slow" alpha (higher and lower frequency, respectively) (Klimesch, 1999). Generally, the alpha peak frequency is lower at frontal electrodes than at occipital electrodes. Frontal-occipital frequency differences in alpha peaks can result in overlapping double peaks ("split-alpha"), which are distinguishable given a sufficiently large frequency difference. Split alpha peaks have been found to occur in the healthy population (Chiang et al., 2008, 2006), and arise naturally in a theoretical model of the generation of the alpha rhythm (Robinson et al., 2003). Additional rhythms in the alpha band are "central alpha" or rolandic mu rhythm from the sensorimotor cortex, and tau rhythm from the auditory cortex (Niedermeyer and Lopes da Silva, 2004), which might be related to a "third" rhythm discovered by Niedermeyer (1997). As with conventional alpha, which is blocked by visual stimuli, mu and tau rhythms are blocked by movements and auditory stimuli, respectively. The "third" rhythm is blocked by cognitive activities but not consistently by auditory stimuli. Another alpha-like rhythm is the theta -band rhythm seen in children when drowsy (Binnie, 2003). These rhythms all behave similarly, by being blocked by cognitive tasks, so can all be thought of as alpha rhythms, which potentially contribute to the traditional alpha band – each differently modulated by experimental conditions and associated with a particular region of the brain (Samson-Dollfus et al., 1997). In contrast, a theta rhythm (at 7–8 Hz) can be evoked by memory activation tasks (Jensen and Tesche, 2002). As such, it is unlikely to occur in resting experimental conditions that favor alpha generation, so will not be confused with alpha. Likewise, pathological theta rhythm is not expected in healthy subjects.

There have been mixed reports of sex differences of the alpha rhythm in the healthy population. Matthis et al. (1980), Díaz de León et al. (1988), Harmony et al. (1990), and Benninger et al. (1984) found significant differences between males and females. Girls were found to have a maturational lag in the increase of alpha frequency in EEG compared with boys, which disappears around adolescence (Clark et al., 2004). Some studies have suggested earlier maturation in girls (Petersén and Eeg-Olofsson, 1971), while others failed to find differences between male and female alpha frequency in EEG (Cohn et al., 1985).

In this paper we examine sex and developmental/aging trends in the alpha rhythm over a wide range of ages, in a sample of 1498 subjects with roughly equal proportions of males and females. A relatively large number of subjects in the range 6–20 years allows detailed examination of age and sex differences during childhood and adolescence, when developmental neurological changes are rapid. The age range extends to 86 years, thus also allowing examination of the later phases of maturation and aging. Despite the concentration at young ages, the number of subjects in the older age range is significantly larger than in most comparable studies.

For processing the large number of subjects involved, we use our recent automated method for the characterization of alpha peaks (Chiang et al., 2008), which has the advantages of being objective and reproducible compared to traditional methods. The method analyzes spectra in two stages: first, spectra from individual sites are fitted; second, information is used from the first stage analysis at multiple electrodes to produce a reduced set of peak parameters that are spatially consistent across electrodes. Several studies have indicated that the EEG is not stationary (Kaplan Alexander et al., 2005, 2004). The use of power spectra over entire recording length results in the loss of all information about phase and any non-stationarity of alpha, and so this method is not directly useful for some questions, but should be seen as complementary to time-domain methods. It is specifically designed to deal with cases of multiple alpha peaks, which have partially distinct spectra and/or spatial distributions. This technique avoids visual bias, integrates spatial information, and can be scaled up to large groups of subjects.

The remainder of this paper is organized as follows: Section 2 briefly outlines the data collection methods, and the algorithm used to determine alpha peak parameters; Section 3 describes age trends and sex differences in these parameters; and Section 4 discusses the implications of these findings.

2. Methods

In this section we present details of the acquisition and processing of the data. Sections 2.1 and 2.2 describe the subject demographics and EEG collection procedure, respectively. Sections 2.3 and 2.4 illustrate the automated algorithm used to extract peak parameters from spectra. Additional details on the peak-fitting algorithm can be found in Chiang et al. (2008). Section 2.5 describes the statistical analysis.

2.1. Subjects

The EEG recordings used in this study were obtained from the BRAINnet website (www.brainnet.net), and are a subset of the Brain Resource International Database, an archive of electrophysiological and psychophysiological measures, demographics, and psychometric tests (Gordon et al., 2005). A group of 1498 subjects was used, comprising 735 females and 763 males, ranging from 6 to 86 years of age. Subjects were healthy, without any known history of brain injury, mental illness, substance abuse, psychological, psychiatric, neurological, or genetic disorders, or other medical conditions that could influence the normality of the EEG. Fig. 1 shows the distribution of age in each sex. The large number of sub-

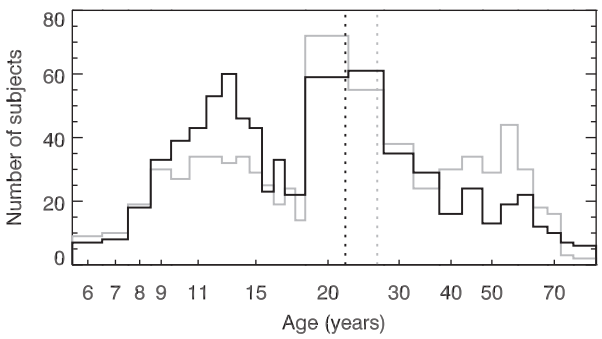

Fig. 1. Histogram of subjects versus age, with single-year bins for ages <20 years, 5-year bins for ages ⩾20 and <80, and a single bin for ages ⩾80 years, which results in a similar number of subjects in each bin. Note the age axis is logarithmic. Female and male subjects are indicated by the gray and black lines, respectively. Mean ages are shown by the vertical dotted lines.

jects in all age bins allows for detailed comparisons between different age and sex groups.

2.2. Recording procedure

Participants were seated in a sound- and light-attenuated room. An electrode cap was used to acquire data from the Fp1, Fp2, F7, F3, Fz, F4, F8, FC3, FCz, FC4, T3, C3, Cz, C4, T4, CP3, CPz, CP4, T5, P3, Pz, P4, T6, O1, Oz, and O2 electrode sites, although only the 19 standard sites in the International 10–20 system for sites were used for further analysis. Subjects were asked to rest quietly with their eyes closed for the two-minute duration of the task. Horizontal eye movements were recorded with electrodes placed 1.5 cm laterally to the outer canthus of each eye. Vertical eye movements were recorded with electrodes placed 3 mm above the middle of the left eyebrow and 1.5 cm below the middle of the left bottom eyelid. A continuous acquisition system (NuAmps), with a sampling rate of 500 Hz, was used in the collection of EEG. Skin resistance was kept below 5 kΩ and a 100 Hz low-pass filter was applied prior to digitization. All scalp EEG channels were referenced to the average of A1 and A2 (mastoids), and were corrected offline for EOG artifact using a technique based on that of Gratton et al. (1983). Average mastoids references were used since they maximizes the amplitude fluctuations observed across all sites.

The EEG time series were first divided into successive 8.192 s segments, which were mean subtracted, windowed, Fourier transformed, modulus squared, and averaged to produce one power spectrum per recording site. Deviations of the EEG in any channel by more than $> \pm 250$ μV from the mean caused the segment to be rejected prior to transformation, because such extreme potentials indicate artifacts. In 42 recordings all 15 segments were rejected by this criterion (see Fig. 2), causing those subjects to be eliminated, and leaving 1456 subjects for further analysis. The distribution of the rejection rate is shown in Fig. 2.

2.3. Peak parameters

The algorithm analyzes the power spectra for a given subject in two stages, as illustrated in Fig. 3. The first stage uses the parametrized spectral form:

$$\log_{10}P(f) \approx E_1 \exp\left(\frac{-(f-f_1)^2}{w_1^2}\right) + E_2 \exp\left(\frac{-(f-f_2)^2}{w_2^2}\right) + G - H\log_{10} f, \quad (1)$$

where f is measured in Hz. In Eq. (1) Gaussian peaks are parametrized by amplitudes E_n, central frequencies f_n, and widths w_n, where the subscript n denotes the peak of interest. This form is numerically fitted over an expanded alpha range (4–14 Hz) of each of the experimental EEGs. The parametrized spectrum includes a power-law background component:

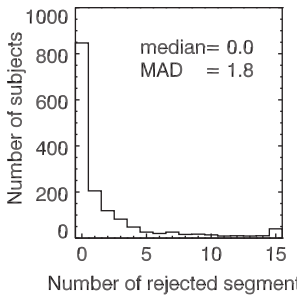

Fig. 2. Histogram of number of segments rejected in each subject. Median and mean absolute deviation (MAD) are shown.

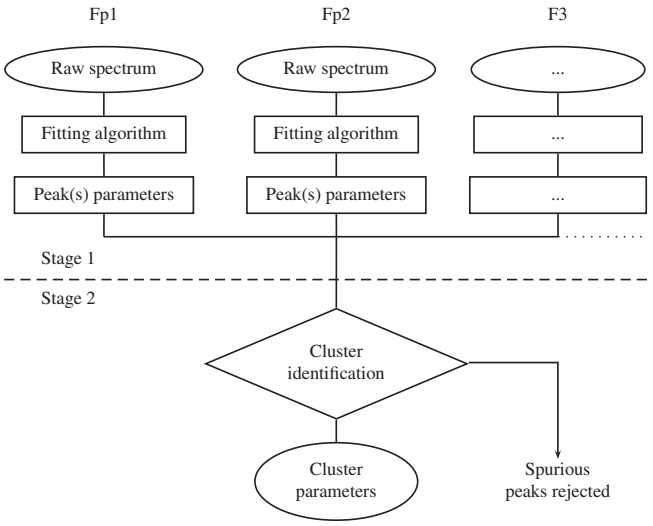

Fig. 3. Schematic showing the stages involved in the estimation of cluster parameters. Stage 1 involves the fitting of individual sites to Eq. (1), and extracting the peak parameters. These parameters are collated, refined, and analyzed collectively in stage 2 to produce the cluster parameters. The final cluster parameter are what is being examined in this paper. Further details can be found in Chiang et al. (2008).

$$P_{bkg}(f) = 10^{G-H\log_{10}f}, \quad = 10^{G}f^{-H}, \quad (2)$$

where 10^G is the normalization and H is the index of the power-law. The absolute amplitude L_n of the peak n is given by:

$$L_n = 10^{E_n+G-H\log_{10}f_n}, \quad (3)$$

and we can define amplitude of the peak corrected for background power to be:

$$K_n = L_n - P_{bkg}(f_n). \quad (4)$$

The second stage selectively collates these fits across all the sites, to rule out noise and to identify robust alpha peak "clusters". A cluster comprises a set of spatially contiguous and spectrally similar alpha peaks. In practice either 0, 1, or 2 clusters are found to be adequate to account for observations. Advantages of this technique include avoidance of visual bias, integration of spatial information, and the ability to handle large amounts of data. Further details of the algorithm are found in Chiang et al. (2008).

Fig. 4 illustrates the results of the fitting algorithm. Fig. 4a shows fitted parameters associated with an individual spectrum. Note that the heights E_n are measured relative to the power-law background. Fig. 4b indicates how clusters were identified. Seven schematic spectra from different recording sites are plotted, with one site (black line) lacking the peak at f_1, and several sites having smaller peaks that were discarded. Criteria are applied in the frequency and spatial domains to extract a small number of clusters from the set of spectral fits (Chiang et al., 2008). In practice, this results in no more than two clusters. For the case with two clusters, the clusters may or may not be spatially overlapping; i.e., spectra may or may not contain two peaks at any particular site.

2.4. Cluster parameters

Once identified, the main characteristics of each cluster can be compactly described by only a few parameters: frequency, position, spatial extent, and average peak power. In this section we give precise definitions for these quantities.

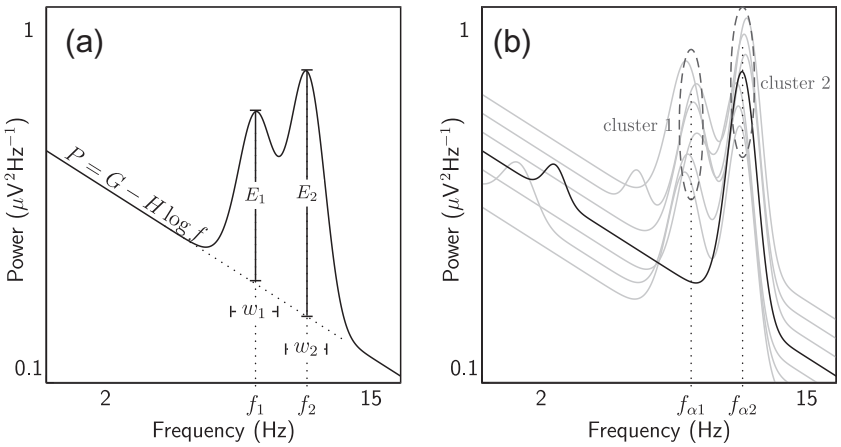

Fig. 4. Illustration of spectral fits. Both axes are shown in logarithmic scale. (a) Schematic of the fitted values for one recording site. (b) Schematic of clustering in a spectrally consistent manner, with lines representing spectra from different sites.

The frequency f of each cluster is defined as the mean frequency of its constituent peaks. The value of f may in principle fall anywhere in the range of frequencies used by the algorithm (4–14 Hz). The weighted occipitality X of a cluster is defined as a sum of the position of its constituent peaks weighted by their corrected amplitude K_n. The location of an electrode corresponding to the location of Fpz (in between Fp1 and Fp2) is defined as $X = 0$ and that of Oz as $X = 1$. The parameter X allows us to distinguish frontal and occipital alpha peaks, and intermediate cases where relevant. The laterality Y of a cluster is defined similarly to X, with the leftmost electrode defined to be at $Y = -0.4$ and the rightmost electrode defined to be at $Y = 0.4$, retaining the difference of 0.2 between closest adjacent electrodes as is defined for occipitality. The spatial extent s is determined as the number of sites displaying at least one peak from the cluster. The value of the cluster size s lies in the range 4–19; the lower bound arises because any cluster with a peak visible in fewer than 4 sites is not considered robust. The average peak power P is taken to be the average value of K_n (see Eq. (4)) within the cluster.

2.5. Curve fitting and statistical analysis

In this section we discuss two specific curve fitting methods that were used in this paper. Section 2.5.1 describes the fitting of smooth asymptotically linear functions to quantify age trends. Section 2.5.2 considers the distribution of frequency differences between clusters for two-cluster cases, to which a Gaussian function is fitted.

2.5.1. Age trend fitting

Age trends were approximated using a functional form that was chosen based on the following observations: (i) some parameters show non-normal distributions; (ii) the median typically shows approximately linear trends at young and old ages; (iii) there was substantial variation in the age ranges over which trends were nonlinear; (iv) the transition from "development" to "aging" occurs gradually, with intermediate slopes in early adulthood; and (v) the median never showed more than one clear turning point for any of the parameters. This motivated a fitting function that is smooth, asymptotically linear, and has a second derivative of constant sign. A functional form that meets these criteria and has only a small number of parameters is given in van Albada et al. (2010):

$$y = Cx + (C - A)\tau \log\left(1 + \exp[-(x - I)/\tau]\right) + D, \quad (5)$$

$$I = \frac{B - D}{C - A}, \quad (6)$$

where x is the age, τ is a width parameter quantifying the age range over which the slope changes considerably, and A, B, C, and D are free parameters. Since fits were relatively insensitive to τ, this parameter was fixed at 3 years, which yielded good fits. Eq. (6) represents a smooth interpolation between two straight lines, $y = Ax + B$ for $x \to -\infty$ and $y = Cx + D$ for $x \to \infty$. These lines intersect at I, the breakpoint age, which is also the point of maximum rate of change in slope for the interpolated fit. Fig. 5 illustrates the functional form.

In order to track the median rather than the mean, fits were performed by minimizing the mean absolute difference (MAD), rather

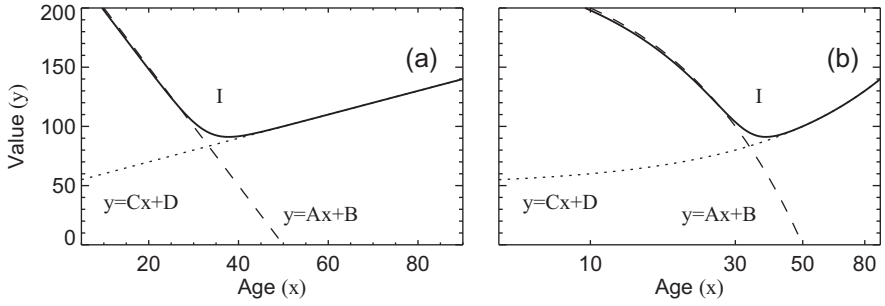

Fig. 5. Example of the function given by Eq. (6) with negative A and positive C (solid line). The asymptotic linear trends $y = Ax + B$ (dashed) and $y = Cx + D$ (dotted) intersect at $x = I$. The linear graph is shown in (a), and (b) shows the age axis logarithmically for later comparisons.

than squared deviations, between fitted and measured values. Optimization was achieved using a downhill simplex method (Nelder and Mead, 1965), with starting conditions determined by linear least-square fits to the age ranges 6–15 and 40–86 years. Confidence intervals for the variables and fits were obtained by bootstrapping with 1000 resamplings.

2.5.2. Gaussian fits

The distribution of alpha frequencies was well described by a Gaussian (see Section 3.1). Since the distribution obtained by subtracting the variates from two independent Gaussian distribution with arbitrary means and variances is also Gaussian, the difference Δf for double-peak cases is also expected to follow a Gaussian distribution. However, the distribution actually obtained may be different, due to cases with unresolvably small Δf being misidentified as single-peak cases. To check whether this occurred, we fitted a Gaussian to the histogram of Δf, taking into account only (positive or negative) values of Δf, for which resolvability of the two peaks was good. The difference between this theoretical Gaussian distribution and the actual distribution of Δf represents cases that theoretically have two closely spaced peaks but in practice may be classified as having a single peak. The number of such cases was compared with the actual number of single clusters found. A confidence interval for the number of cases potentially misidentified as having a single peak was obtained by bootstrapping with 1000 resamplings.

The cutoff values of Δf for the Gaussian fit were chosen based on the following considerations: (i) taking a large cutoff could leave insufficient data to produce a reliable fit, and (ii) taking a small cutoff would underestimate the number of cases incorrectly classified as having a single peak. The compromise used in this paper is to take the Δf corresponding approximately to the peaks of the bimodal histogram as the cutoff values.

3. Results

First, we discuss the removal of outliers from the data. Second, we examine various ways of differentiating between clusters. Third, age trends of the cluster alpha parameters are presented. Finally, the cluster parameters are examined for sex differences.

3.1. Parameter distributions and outliers

Our algorithm examines an expanded alpha range (4–14 Hz) to accommodate the known variations of alpha frequency with age (in particular, lower alpha frequency in childhood and adolescence). The algorithm attempts to distinguish true alpha peaks from noise by using several morphological criteria, however this filtering stage is less effective near the extremes of the chosen frequency range, due to less constrained curve fits. In this section we identify these cases and eliminate them from our subsequent analysis.

The algorithm described in Section 2.3 was applied to 1456 subjects, with 42 others rejected for having excessively noisy EEG spectra. Each of these yielded either zero, one, or two sets of cluster parameters (*f, X, Y, s*, and *P*), of which only *f* and *X* were used in outliers rejection. Fig. 6 shows the distribution of the occipitality *X* of each cluster against its averaged frequency *f*, with the color of each point indicating the cluster type. The majority of the points are grouped in a central band. Other than the central grouping we see two distinct groups of points: (a) a group of points with $f < 5$ Hz, distinct from the central band of clusters, and (b) a second group of points with $f > 13$ Hz, which show less distinct separation from the central band. The points near the two frequency limits (4 and 14 Hz) do not appear to follow the linear trend displayed by the central group of points; hence these probably represent outliers. We can identify the outliers by frequency cutoffs at 13 Hz and 5 Hz. After removing outliers, there were 41 subjects with no discernible clusters, 744 subjects with one cluster, and 671 subjects with two clusters, as listed in Table 1. Fig. 7 illustrates the distribution of clusters for male and female subjects in each age bin after the elimination of the outliers. The remaining peaks are referred to hereafter as 'alpha', even when they fall in the traditional theta band, since the experimental conditions make this label the most plausible.

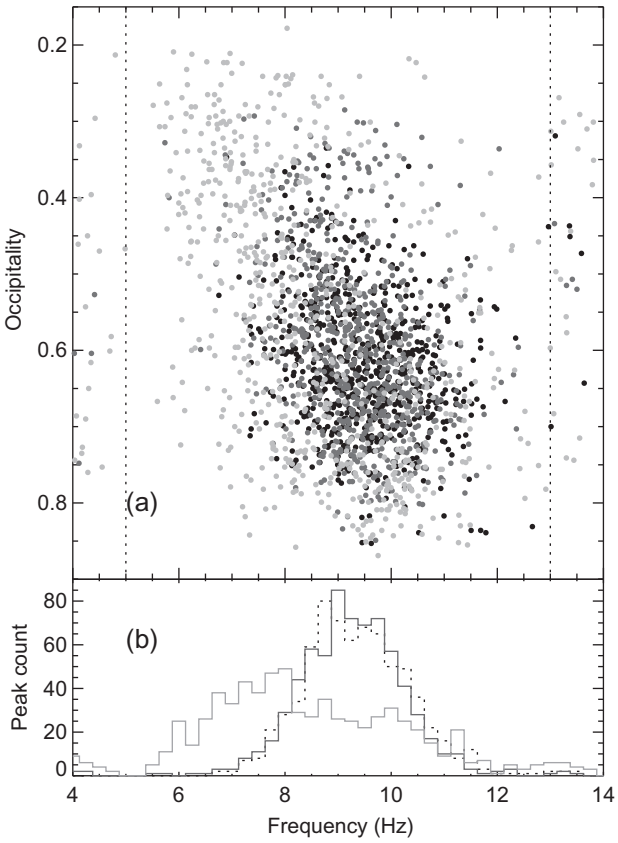

Fig. 6. Scatter plot of alpha peak clusters in the *f*–*X* plane, with the top of the diagram indicating the front of the head. (a) Black, dark gray and light gray circles, respectively, denote one-cluster peaks, peaks of higher spatial extent from the two-cluster case, and peaks of lower spatial extent from the two-cluster case. The dotted lines show the upper and lower constant frequency cutoff. (b) Histogram of the frequency distribution of peaks. The dotted line represents one-cluster peaks, while the dark and light gray solid lines correspond to the peaks of higher and lower spatial extent from the two-cluster case, respectively.

In what follows the clusters are distinguished by their relative occipitality *X*, with higher occipitality defining the occipital cluster, and the lower occipitality defining the frontal cluster. The relation between the frontal and occipital frequency is plotted in Fig. 8a.

Table 1
Breakdown of number of alpha clusters per subject after removal of outliers. *N* denotes subjects whose EEG was discarded prior to analysis because of excessive time-series noise.

Number of alpha clusters	Female	Male	All subjects	Percentage
N	24	18	42	2.8
0	24	18	42	2.8
1	356	395	751	50.1
2	331	332	663	44.3
Number analyzed (0 + 1 + 2)	711	745	1456	97.2
Total	735	763	1498	100.0

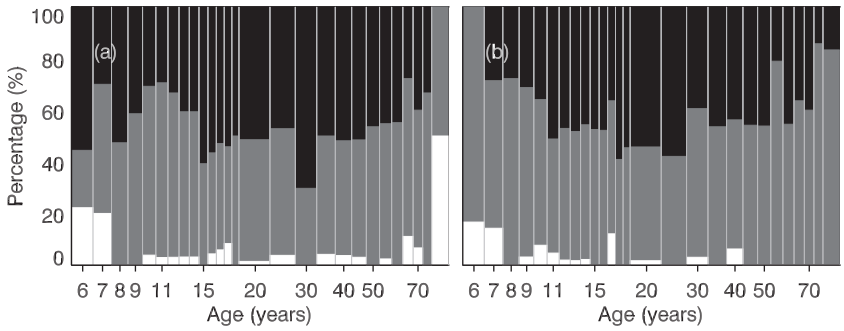

Fig. 7. Percentage of alpha peak clusters in each age bin, as in Fig. 1. White corresponds to the case with no peak cluster, dark gray to the one peak cluster case, and black to two peak clusters. (a) Females. (b) Males.

When $f_F \approx f_O$ the peaks cannot be resolved; hence, there is a gap close to the dotted line representing $f_F = f_O$. If the frontal frequency is higher than that of the occipital frequency it would be located above the $f_F = f_O$ line, and vice versa. Although a significant fraction (22%) of the points are above the line of equality ($f_F = f_O$), most subjects have a higher occipital cluster frequency compared to that of the frontal cluster, as found previously (Rubin Morton, 1938).

The relative powers of the frontal and occipital alpha peaks are shown in Fig. 8b. We can see the distribution of the power is skewed towards a higher occipital peak, as reported in the literature (Inouye et al., 1986), with occipital alpha dominant. However, in approximately 26% of the cases the frontal power is higher than the occipital power.

Fig. 8c shows whether the frequency ratio and relative power of the two peaks are correlated. While there is a broad scatter, a clear positive correlation is seen. Specifically, higher relative occipital frequency is correlated with a higher relative occipital power, as seen in the denser clustering of points toward the top right and bottom left corners.

The distributions of parameters *f, X, Y, s*, and *P* are shown in Fig. 9. In all three cases (one alpha cluster and both of the two alpha clusters cases) (i) *X* tends to be more occipital than frontal, (ii) $|Y| \ll 1$ reflects small lateral differences, and (iii) the frequency distribution is centered at approximately 10 Hz. Compared with the one-cluster cases, the two-cluster cases have (i) a greater proportion of clusters at low frequencies (left side of Fig. 9*f*2), (ii) a wider range of positions along the frontal-occipital axis (left and right sides of Fig. 9*X*2), (iii) a greater proportion of clusters extending across a small number of electrodes (left side of Fig. 9*s*2), and (iv) a greater proportion of clusters having smaller cluster average peak power (left side of Fig. 9*P*2). When the two-cluster parameter values are split into two separate distributions (where we arbitrarily choose to split by spatial extent), we find that those distributions describing the cluster of *larger* spatial extent (solid line in row 2 of Fig. 9) resemble the one-cluster distributions (row 1 of Fig. 9).

3.2. Cluster order

The similarity and differences between the one- and two-peak cases in Fig. 9 suggest that – where two peaks can be distinguished – one is approximately as in the single peak case, while the other is lower in frequency, more frontal, and smaller in extent and power. However, it is not possible to conclude this from Fig. 9 alone, as we cannot infer whether or not all these distinctions are correlated. The following sections thus examine the same set of values as in Fig. 9, but after classification by "cluster order", and with the aid of the independent variables of age and sex.

To understand better the contrasting distributions in Fig. 9 it helps to distinguish the members of each two-cluster pair. Member clusters can be labeled by their (a) cluster average frequency *f*, (b) cluster occipitality *X*, (c) cluster spatial extent *s*, or (d) cluster averaged peak power *P*. The laterality parameter *Y* has been omitted here due to left-right near-symmetry, but is explored in Section 3.4.3. We examine these alternatives below.

Differentiating clusters by their relative (a) *f* corresponds to separation into cases of fast and slow alpha, (b) *X* corresponds to separation into occipital and frontal alpha, (c) *s* corresponds to separation by spatial extent, as measured by the number of electrodes at which each cluster is discernible (Chiang et al., 2008), and (d) *P* corresponds to separation by the relative strengths of peaks in the clusters. Here we define the "upper" cluster to be the cluster whose differentiating parameter (i.e., *f, X, s*, or *P*) has a higher numerical value than that of the "lower" cluster.

To further examine the association between the alternative cluster ordering we constructed the contingency tables and calculated the associated Fisher exact probabilities. See Table 2. The contingency table is used to record the relations between the parameters pairwise, and the Fisher exact test is used in the analysis of the contingency table to examine the significance of the association between classifications. The parameter *s*, representing the spatial extent of the cluster, is not associated with any of the parameters, potentially due to the top (19 electrodes) or the bottom (4 electrodes) bounds from the algorithm. Laterality is also only weakly associated with the other parameters. The other three parameters, *f*, *X*, and *P*, are all highly associated with each other, showing the corresponding cluster orderings are very similar.

3.3. Age trends

Here we examine the same alpha cluster parameters as shown in Fig. 9, but as functions of both age and each of the four classification options described above.

Fig. 10 shows comparisons between each of the four ways to examine alpha cluster parameters, with age variations, by cluster order. To classify the trends, cluster parameters of subjects were averaged within each of the age bins; and this averaging is denoted by angled brackets, $\langle\ \rangle$. The single cluster trend is shown in these figures, together with both the "upper" and "lower" clusters of the two-cluster case, for each of the four parameters (*f, X, s*, or *P*). For two-cluster cases, the upper and lower cluster age trends are roughly consistent in all subpanels in all four figures, which shows that to a large extent the four alternative cluster orderings are interchangeable. Nevertheless the clearest separation of the upper and lower clusters of the two-cluster case versus any parameter occurs, by definition, when the classification of the groups are determined by the said parameter: these cases are seen in Fig. 10a, f, k, and p. The one-cluster cases are the same in all four frames and serve as a comparison to the two-cluster cases.

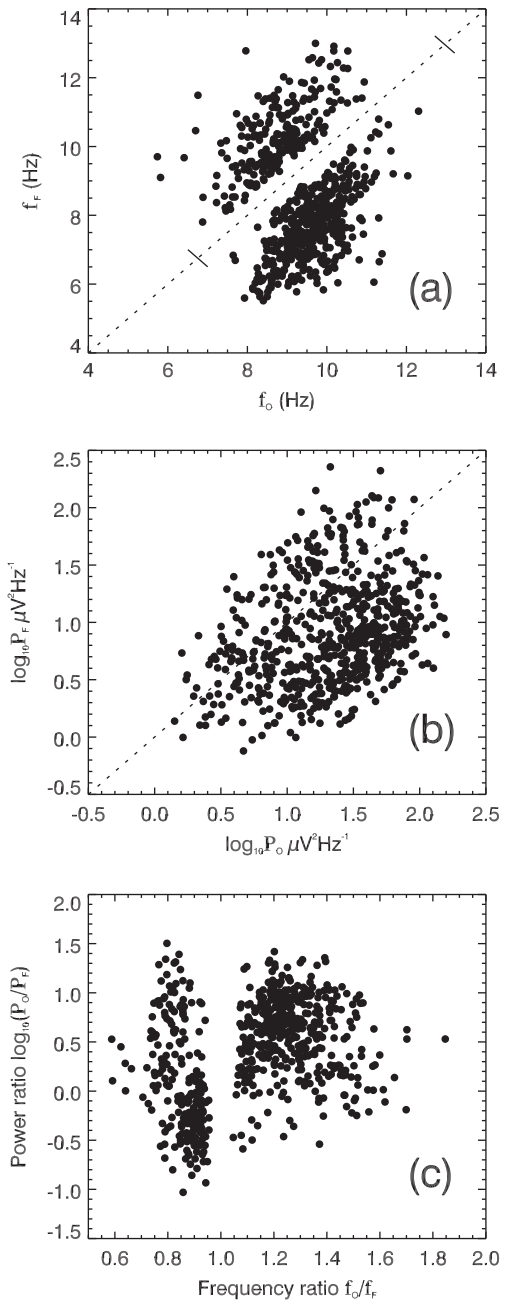

Fig. 8. (a) Frontal alpha frequency f_F versus occipital alpha frequency f_O in two-cluster cases. The dotted line shows $f_F = f_O$. The transverse marks across the dotted line indicate the upper and lower bounds of the frequencies of one-cluster cases. (b) Frontal alpha power (P_F) versus occipital alpha power (P_O) in two-cluster cases. The dotted line shows $P_F = P_O$. (c) Relationship between the frequency ratio (f_O/f_F) and the power ratio (P_O/P_F). A gap at $f_O/f_F = 1$ is due to the lack of resolvability between the two peaks if the frequencies are nearly the same.

We found $\langle f \rangle$ (first row of Fig. 10) to have a clear age trend. Single clusters $\langle f \rangle$ are consistent with the trend widely reported in the literature, with the alpha frequency increasing up to approximately age 20, and decreasing gradually during adulthood (Niedermeyer and Lopes da Silva, 2004). The single peak trends roughly match those of the upper of the two clusters: the higher-frequency member (Fig. 10a), the more occipital member (Fig. 10b), the member with greater spatial extent (Fig. 10c), and the member with a greater maximum peak power (Fig. 10d). Both lower and upper cluster frequency shown in Fig. 10a, and corresponding roughly to the frontal and occipital alpha, respectively in Fig. 10b, continue to increase in late adulthood, in clear contrast with the one-cluster case.

A clear age trend was also observed in mean occipitality $\langle X \rangle$. For one-cluster, and for both upper and lower peaks of the two-cluster cases, there is a consistent decrease of $\langle X \rangle$ with age, indicating that clusters become more frontal with age. This is somewhat surprising in view of age-related increases in frequencies for cases with two clusters, and the generally lower alpha frequencies at frontal sites. Fig. 10g shows that there is no clear correlation between cluster size and occipitality.

The spatial extent $\langle s \rangle$ shows an overall upward trend with age. The upper and lower clusters are least distinct when the classification is based on X (Fig. 10j) again indicating that frontal and occipital clusters extend across comparable numbers of sites. When the classification is based on frequency, the separation of the upper and lower clusters is most distinct at younger ages and less clear at older ages.

The peak power $\langle P \rangle$ is high during early adolescence and declines until approximately age 20, after which the trend levels off for the one-cluster case. The downward trend is persistent in adulthood for both upper and lower two-cluster cases. The separation of the upper and lower clusters in the two-cluster case is quite clear for all the parameters, as seen in the final row of Fig. 10.

In Fig. 10, for the two-cluster cases, the value of the variable plotted for the upper cluster is higher on average than that for the lower cluster. This shows that all four classification are correlated; i.e., the second peak has lower frequency, is more frontally located, has a smaller spatial extent, and has less power.

3.4. Sex differences

This section examines parameter differences between males and females. We first look at the one-cluster case, since it shows the strongest age trends. Second, we examine two-cluster cases classified according to occipitality X to enable a comparison between frontal and occipital alpha peaks. Finally we examine differences in laterality Y. In this section we present two types of result. Fits of Eq. (6) are shown in Tables 3 and 4. The fits are also presented graphically in Fig. 11.

3.4.1. One-cluster cases

The fits to one-cluster age trends are shown in Table 3 and the first column of Fig. 11. The similarity in age trends between males and females is demonstrated by the overlap of their respective 95% confidence band in Fig. 11, as well as by the values in Table 3. There was a significant increase in f during development in both males and females, while the subsequent decrease was clearest in females. We can see in the median fit values inFig. 11a that females have a significantly lower alpha frequency compared to males prior to around age 16 (which is approximately the breakpoint age). Median frequencies for male (f_m) and female (f_f) subjects are 9.44 and 9.38 Hz, respectively (Mann–Whitney $U = 14361$, $n_m = 184, n_f = 141$, $P < 0.05$, alternative hypothesis: $f_m > f_f$). The trend is reversed during early adulthood, approximately the age of 40, during which f_m and f_f are 9.66 and 9.85 Hz, respectively ($U = 6580.5$, $n_m = 132, n_f = 113$, $P = 0.06$, alternative hypothesis: $f_m < f_f$). After that, f_m and f_f are 9.19 and 9.01 Hz, respectively ($U = 4494.5$, $n_m = 79, n_f = 102$, $P = 0.09$, alternative hypothesis: $f_m > f_f$).

Fig. 11d shows that X continues to become more frontal throughout the age range in females, whereas in males it moves more occipitally from about age 40 years onward. Only the male negative asymptotic slope prior to the breakpoint age reached significance (see Fig. 11d and Table 3).

Fig. 11g shows that for the spatial extent s, females have stronger age trends than males, although both curves are close to the upper bound of 19 electrode sites. This indicates that, if a single cluster is present, it generally extends across all electrodes examined.

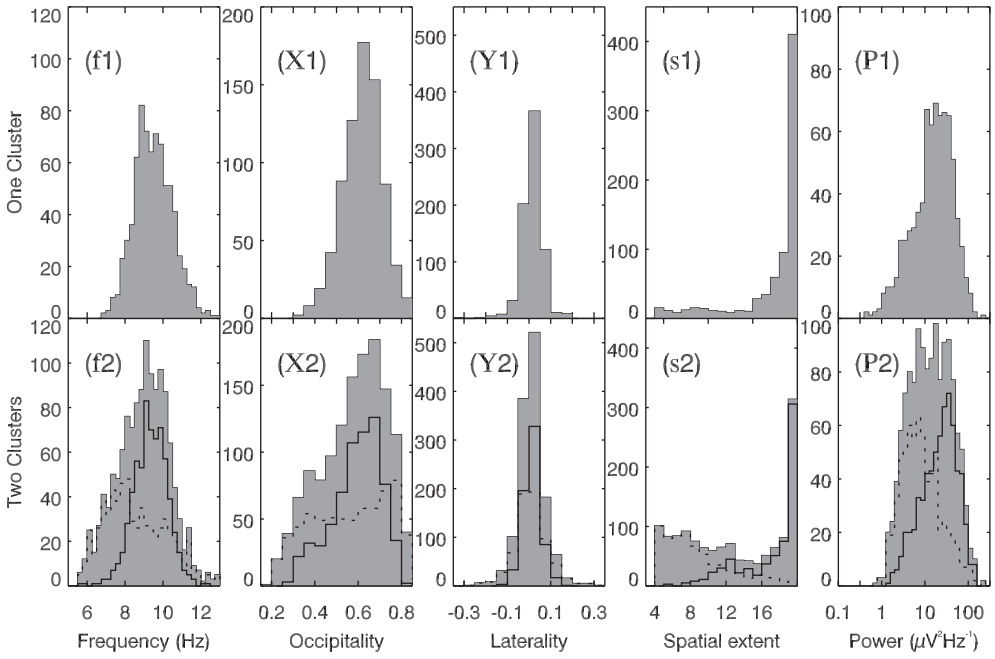

Fig. 9. Histograms of parameters: alpha peak frequency *f*, cluster average occipitality *X*, cluster average laterality *Y*, spatial extent *s*, and cluster averaged peak power *P*. Results for the 751 subjects with one alpha cluster are shown in the upper row, and those for the 663 subjects with two clusters are shown in the lower row. In the latter case, the 663 pairs of values are plotted as two separate histograms: one showing the distribution of values (*f, X, Y, s*, or *P*) associated with the *spatially smaller* cluster (dashed line); and one showing the distribution associated with the *spatially larger* cluster (solid line). The sum of the two histograms is also plotted (shaded).

Finally, *P* decreases to a lower level in males than in females in early adulthood (≈16), with median power for male (P_m) and female (P_f) subjects equal to 26 and 18 $\mu V^2\,Hz^{-1}$, respectively ($U = 14382.5$, $n_m = 184, n_f = 141$, $P < 0.05$, alternative hypothesis: $P_m > P_f$). Furthermore, both males and females showing a significant negative slope prior to the breakpoint age shown in Fig. 11j and Table 3. Note that the slopes of *P* are fitted on a logarithmic scale because of the big variations in *P*.

3.4.2. Two-cluster cases

Since a clearly superior choice of the cluster ordering did not present itself, we examine ordering of two-clusters only by occipitality. Columns two and three in Fig. 11 illustrate the two-cluster fits with uncertainties, where clusters were ordered according to their occipitality *X*. Hence upper and lower clusters correspond to the occipital and frontal location, respectively. The parameters of the corresponding fits are listed in Table 4.

In Section 3.1 for males and females combined, the parameter *f* neither of the two clusters seen in Fig. 10b shows the clear frequency reduction in adults that is apparent in the one-cluster cases. With the separation of the sexes we note that the occipital frequency (Fig. 11b) shows a similar trend to the one-cluster case, but much weaker and not statistically significant. The frontal frequency (Fig. 11c) however shows an increase over almost the whole age range. This discrepancy arises from the high variability in the dataset, with Fig. 10 showing an age averaged value whereas Fig. 11 shows the median of bootstrapped fits. Table 4 shows that the positive asymptotic slope for the upper cluster reached significance only when both sexes were combined prior to the breakpoint age. No post-breakpoint slopes for *f* reached significance.

For *X* we showed that in Fig. 11e the occipital (upper) cluster becomes more frontal until approximately the breakpoint age (≈20) and remains stable afterwards in both sexes. In Fig. 11f, the frontal (lower) cluster occipitality levels off in males after age 40 years, but continue to become more frontal in females. Only the slope for the upper (occipital) cluster in the all-subjects group prior to the breakpoint age reached significance (Table 4).

Figs. 11h and i show the changes in spatial extent for occipital and frontal clusters, respectively. For both sexes the occipital cluster appears to become smaller after age 20, whereas the frontal cluster remains relatively stable throughout the age range. However, none of the asymptotic slopes for this parameter reached significance.

The average peak power *P* of the frontal cluster shown in Fig. 11l is similar to that in the one-cluster case in both sexes, with males showing a clearer breakpoint age compared to females, and having higher power prior to adolescence: median powers for male (P_m) and female (P_f) subjects are 38 and 29 $\mu V^2\,Hz^{-1}$, respectively ($U = 8552$, $n_m = 145, n_f = 102$, $P < 0.05$, alternative hypothesis: $P_m > P_f$). A consistent reduction in average peak power *P* for both sexes in the occipital cluster is apparent in Fig. 11k.

Table 2
Contingency table and Fisher exact test for association of the parameters in the two-cluster case. The values above the diagonal show the contingency tables from the classification of the "upper" and "lower" cluster (U and L, respectively) by the parameter of interest. The symbols below the diagonal show the probability of non-association. The symbols $**$, $*$, and *n.s.* represent the significance of association is $p \ll 0.005$, $0.05 < p < 0.5$, and $p \approx 1$, respectively. The diagonal entries are omitted.

		f		*X*		*Y*		*s*		*P*	
		U	L	U	L	U	L	U	L	U	L
f	U	–		345	89	246	188	433	1	401	33
	L			49	180	114	115	229	0	109	120
X	U	**		–		226	168	393	1	369	25
	L					134	135	269	0	141	128
Y	U	*		*		–		359	1	284	76
	L							303	0	226	77
s	U	*n.s.*		*n.s.*		*n.s.*		–		509	153
	L									1	0
P	U	**		**		*		*n.s.*		–	
	L										

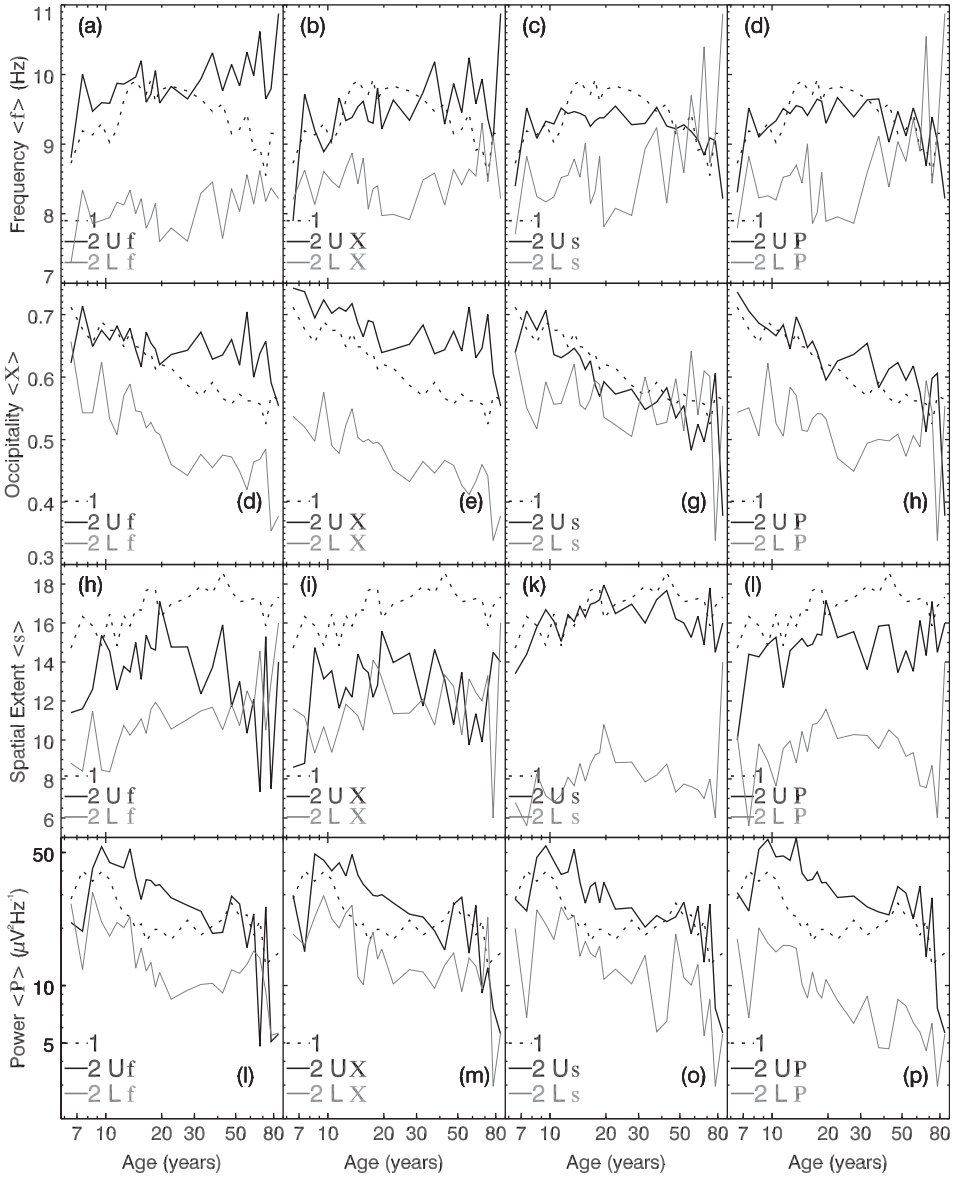

Fig. 10. Subject cluster parameters averaged in age bins versus age (with age bins as indicated in Fig. 1). The averaged frequency $\langle f \rangle$, occipitality $\langle X \rangle$, spatial extent $\langle s \rangle$, and cluster average peak power $\langle P \rangle$ are in first, second, third, and fourth row, respectively. Dotted lines denote the single alpha cluster subjects. The solid lines denote the two-cluster cases, with black the upper and gray the lower clusters. Columns correspond to the method of classification of clusters. The first column (a) shows paired clusters classified by *f*; in the second (b), third (c), and fourth column (d) the clusters are classified by *X*, *s*, and *P*, respectively. Rows correspond to the respective parameters of interest labeled on the left hand side of the frames. The dotted lines (cases for which only one cluster was found) in all the plots are identical. Errors are roughly uniform across the age ranges except for the extremes where the numbers of subjects are lower.

3.4.3. Lateral differences

The laterality values are small, as seen in Fig. 9. The parameters of the fitted age trends are listed in Tables 3 and 4. Fig. 12 shows that laterality for both the one-cluster and occipital cluster (Fig. 12a and b, respectively) is mostly right dominated (positive *Y*), with the 95% confidence interval above zero over the range 10–40 years of age for both sexes. The frontal cluster (Fig. 12c) shows less right dominance, and after the age of 40 in the fitted trends shows increasing right and left dominance for the males and females, respectively. The deviation from symmetry is small, with the *Y* value of −0.02 in females corresponds to a lateral deviation of only about 0.8 cm.

3.5. Are single peaks unresolved double peaks?

In a further analysis of the cluster parameters, subjects with only one alpha cluster are compared to those with two distinguishable clusters. This is motivated by the possibility that the distinction between these two group is artificial; i.e., that all subjects have two peaks, and the one-cluster subjects are simply those with unresolved double peaks. This hypothesis is suggested both by parsimony, and by the fact that if a frontal and an occipital cluster have a small enough frequency difference, it is likely that they will be unresolved and thus conflated into one. We explore this idea here by considering the distribution of f_{single} from the one cluster group, and the distribution of $\Delta f = f_{upper} - f_{lower}$ (where f_{upper} and f_{lower} are the frequency of the upper and lower of the two-clusters, respectively) from the two cluster group, where the clusters were ordered by laterality *Y*. Due to the large degree of left-right symmetry of clusters, this ordering leads to a nearly symmetrical distribution of Δf, simplifying the fitting of the Gaussian.

The key idea is that the distribution of Δf for two-cluster cases (Fig. 13a) may be attributable to a simple unimodal distribution, which has a deficit around $\Delta f = 0$ due to those cases being having

Table 3
Results of fitting Eq. (6) to the age trends and mean absolute deviation of the one-cluster case. Parameters *A* and *C*, and *B* and *D*, are the slopes and intercepts pre and post breakpoint age (*I*), respectively. Slopes (parameters *A* and *C*) that significantly deviate from zero at the 95% level are highlighted in bold. Parameters are in their respective units (Hz for *f*, dimensionless for *X*, *Y*, *s*, and $\mu V^2\ Hz^{-1}$ for *P*.)

	A (yrs^{-1})	*B*	*C* (yrs^{-1})	*D*	*I* (yrs)
All subjects					
f	$\mathbf{0.15 \pm 0.04}$	8.0 ± 0.3	$\mathbf{-0.019 \pm 0.004}$	10.2 ± 0.1	14 ± 2
X	$\mathbf{-(5.5 \pm 0.8) \times 10^{-3}}$	0.737 ± 0.009	$-(3 \pm 4) \times 10^{-4}$	0.59 ± 0.03	30 ± 10
Y	$-(2 \pm 2) \times 10^{-3}$	0.020 ± 0.009	$-(1.7 \pm 0.1) \times 10^{-4}$	0.018 ± 0.007	7 ± 20
s	0.2 ± 0.1	16 ± 1	$-(4 \pm 9) \times 10^{-3}$	19.1 ± 0.4	10 ± 50
log*P*	$\mathbf{-0.08 \pm 0.02}$	2.0 ± 0.2	$(0 \pm 1) \times 10^{-4}$	1.17 ± 0.06	11 ± 2
Female					
f	$\mathbf{0.17 \pm 0.06}$	7.7 ± 0.5	$\mathbf{-0.024 \pm 0.003}$	10.4 ± 0.1	14 ± 2
X	$-(2 \pm 2) \times 10^{-3}$	0.68 ± 0.04	$\mathbf{-(2.0 \pm 0.5) \times 10^{-3}}$	0.67 ± 0.04	10 ± 100
Y	$(0 \pm 3) \times 10^{-5}$	0.02 ± 0.01	$-(3 \pm 1) \times 10^{-4}$	0.023 ± 0.005	10 ± 10
s	$\mathbf{0.5 \pm 0.2}$	13 ± 2	$(0 \pm 1) \times 10^{-3}$	19.1 ± 0.5	12 ± 2
log*P*	$\mathbf{-0.1 \pm 0.03}$	1.8 ± 0.3	$-(2 \pm 2) \times 10^{-3}$	1.3 ± 0.1	6 ± 4
Male					
f	$\mathbf{0.15 \pm 0.06}$	8.1 ± 0.3	-0.011 ± 0.006	9.9 ± 0.2	11 ± 6
X	$\mathbf{-(5.5 \pm 0.8) \times 10^{-3}}$	0.74 ± 0.01	$(1.3 \pm 0.6) \times 10^{-3}$	0.48 ± 0.04	39 ± 5
Y	$-(5 \pm 3) \times 10^{-3}$	0.03 ± 0.02	$(0 \pm 2) \times 10^{-6}$	0.01 ± 0.02	7 ± 40
s	–	–	$(1 \pm 8) \times 10^{-3}$	18.9 ± 0.7	–
log*P*	$\mathbf{-0.06 \pm 0.01}$	2.1 ± 0.1	$(2 \pm 2) \times 10^{-3}$	1 ± 0.1	17 ± 3

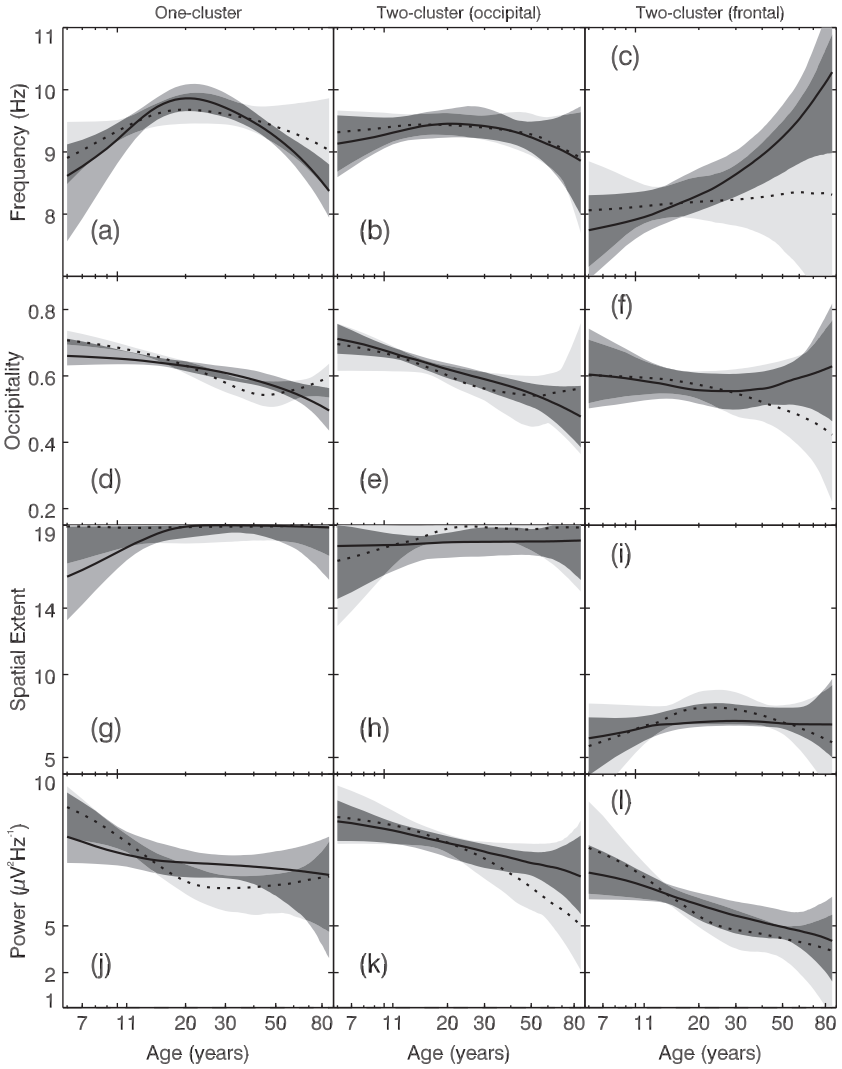

Fig. 11. Fits of the function given in Eq. (6) to the cluster frequency, occipitality, spatial extent, and power in the first, second, third, and fourth row, respectively. The first column shows the one-cluster cases, the second column the occipital clusters, and the third column the frontal cluster cases. The rows shows the parameter of interest. The gray patches represent 95% confidence intervals for the fits, with the lightest shade representing the female subjects, the next shade the male subjects, and the darkest shade the overlapping parts of the plot. The lines trace the medians of the individual fits, with the solid and dotted lines representing the female and male subjects, respectively. Both the confidence intervals and median traces were obtained by bootstrapping.

Table 4
Parameters ($A - D$ and I) and median absolute deviations of age trends of the function given in Eq. (6) for two-cluster cases. Clusters were ordered according to occipitality, so that 'upper' refers to occipital clusters, and 'lower' to frontal ones. Breakpoint ages (I) outside the age range examined (6–86 years), and the associated slope parameters are omitted. Slopes that significantly deviate from zero in the 95% confidence interval are highlighted in bold. Parameters are in their respective units (Hz for f, dimensionless for X, Y, s, and $\mu V^2\ Hz^{-1}$ for P.)

		A (yrs^{-1})	B	C (yrs^{-1})	D	I (yrs)	
All subjects	Upper	f	0.06 ± 0.03	8.9 ± 0.9	$-(9 \pm 4) \times 10^{-3}$	9.7 ± 0.2	10 ± 3000
		X	$-(\mathbf{8 \pm 2}) \times \mathbf{10^{-3}}$	0.76 ± 0.03	$-(4 \pm 6) \times 10^{-4}$	0.57 ± 0.04	20 ± 40
		Y	$(4 \pm 3) \times 10^{-3}$	-0.01 ± 0.02	$-(2 \pm 2) \times 10^{-4}$	0.02 ± 0.02	9 ± 20
		s	0.2 ± 0.1	16 ± 2	$(0 \pm 1) \times 10^{-4}$	18.2 ± 0.6	10 ± 600
		$\log P$	-0.011 ± 0.01	1.8 ± 0.3	$-(5 \pm 4) \times 10^{-3}$	1.4 ± 0.3	20 ± 2000
	Lower	f	0.06 ± 0.05	7.9 ± 0.7	0.02 ± 0.01	8.0 ± 0.7	7 ± 200
		X	–	–	$-(3 \pm 9) \times 10^{-4}$	0.58 ± 0.03	–
		Y	$(0 \pm 4) \times 10^{-4}$	0.03 ± 0.02	$-(1 \pm 5) \times 10^{-4}$	$(0 \pm 3) \times 10^{-3}$	20 ± 20
		s	0.3 ± 0.2	4 ± 2	-0.02 ± 0.02	8.2 ± 0.9	10 ± 90
		$\log P$	-0.03 ± 0.02	1.5 ± 0.2	$-(3 \pm 4) \times 10^{-3}$	0.8 ± 0.2	20 ± 60
Female	Upper	f	0.04 ± 0.04	9 ± 1	-0.011 ± 0.007	9.7 ± 0.3	10 ± 400
		X	$-(9 \pm 4) \times 10^{-3}$	0.77 ± 0.04	$-(1.9 \pm 0.7) \times 10^{-3}$	0.64 ± 0.03	20 ± 70
		Y	$(0 \pm 4) \times 10^{-6}$	0.02 ± 0.01	$-(2 \pm 4) \times 10^{-4}$	0.02 ± 0.03	10 ± 6000
		s	$(0 \pm 1) \times 10^{-3}$	17 ± 2	$(0 \pm 1) \times 10^{-3}$	17.9 ± 0.6	10 ± 2000
		$\log P$	-0.02 ± 0.01	1.7 ± 0.1	$-(4 \pm 3) \times 10^{-3}$	1.4 ± 0.2	20 ± 2000
	Lower	f	–	–	0.029 ± 0.008	7.7 ± 0.3	–
		X	$-(4 \pm 7) \times 10^{-3}$	0.67 ± 0.09	$(1 \pm 2) \times 10^{-3}$	0.52 ± 0.06	20 ± 70
		Y	$(0 \pm 3) \times 10^{-4}$	0.02 ± 0.03	$(4 \pm 6) \times 10^{-4}$	-0.01 ± 0.02	20 ± 20
		s	0.2 ± 0.2	5 ± 2	$(0 \pm 1) \times 10^{-3}$	7.2 ± 0.5	10 ± 200
		$\log P$	-0.02 ± 0.02	1.4 ± 0.2	$-(3 \pm 4) \times 10^{-3}$	0.9 ± 0.2	20 ± 400
Male	Upper	f	0.07 ± 0.06	9.2 ± 0.7	$-(9 \pm 9) \times 10^{-3}$	9.6 ± 0.5	9 ± 200
		X	$-(7 \pm 3) \times 10^{-3}$	0.74 ± 0.04	$(0 \pm 2) \times 10^{-4}$	0.5 ± 0.3	30 ± 400
		Y	$(8 \pm 5) \times 10^{-3}$	-0.04 ± 0.03	$-(1 \pm 3) \times 10^{-4}$	0.01 ± 0.02	8 ± 20
		s	0.3 ± 0.2	15 ± 3	$(0 \pm 2) \times 10^{-3}$	19.0 ± 0.8	10 ± 200
		$\log P$	-0.01 ± 0.01	1.9 ± 0.8	$-(9 \pm 7) \times 10^{-3}$	1.5 ± 0.6	20 ± 3000
	Lower	f	0.03 ± 0.07	8.0 ± 0.5	$(0 \pm 2) \times 10^{-3}$	8 ± 3	10 ± 60
		X	–	–	$-(3 \pm 2) \times 10^{-3}$	0.6 ± 0.1	–
		Y	$(0 \pm 7) \times 10^{-4}$	0.03 ± 0.02	$-(5 \pm 8) \times 10^{-4}$	0.02 ± 0.06	10 ± 40
		s	0.3 ± 0.2	4 ± 3	-0.04 ± 0.02	8.9 ± 0.9	20 ± 10
		$\log P$	-0.05 ± 0.02	1.7 ± 0.3	$-(3 \pm 4) \times 10^{-3}$	0.8 ± 0.2	20 ± 20

classified as only one cluster. If this is so, the area of the deficit should equal the number of one-cluster cases. The histogram of Δf is shown in Fig. 13a, with a Gaussian fitted to the wings ($|\Delta f| > 1.75$ Hz), and Fig. 13b shows this residue with a Gaussian fit. The 95% confidence interval for the residue is (586, 1078), obtained from fitting a Gaussian to each bootstrap sample and taking the residue. This is consistent with the number of one-cluster cases (671).

4. Discussion

We have examined the alpha spectral peak parameters of a large dataset of healthy subjects of both sexes using a recently developed automated method for peak identification and parametrization (Chiang et al., 2008), which groups alpha peaks at different electrodes according to their spectral similarities. This enabled information from multiple electrodes to be rendered in a manageable format. Parameters extracted for each cluster of alpha peaks were frequency f, occipitality X, laterality Y, spatial extent s, and power P. The variations of these parameters with respect to position, age, and sex were explored.

The main findings of this paper are:

(i) We reproduced several classical results (Niedermeyer and Lopes da Silva, 2004): first the alpha peak is present in most sub-

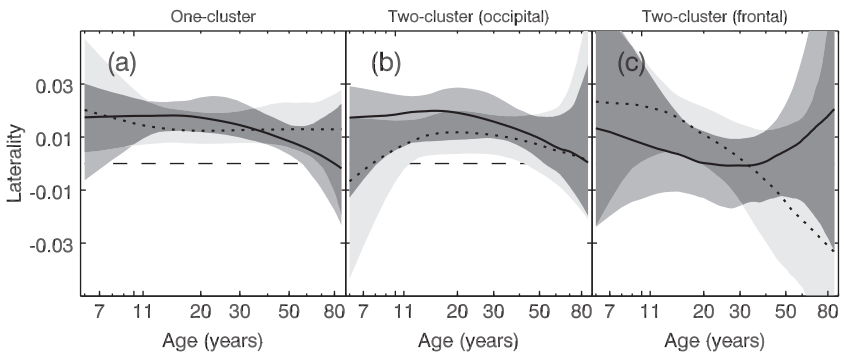

Fig. 12. Changes of laterality Y across age in the same format as Fig. 11, (a) one-cluster case, (b) occipital cluster, and (c) frontal cluster. Positive laterality Y indicates a cluster is right-dominated, where as negative Y indicates a cluster is left-dominated. The zero-line and is indicated by the dashed horizontal lines.

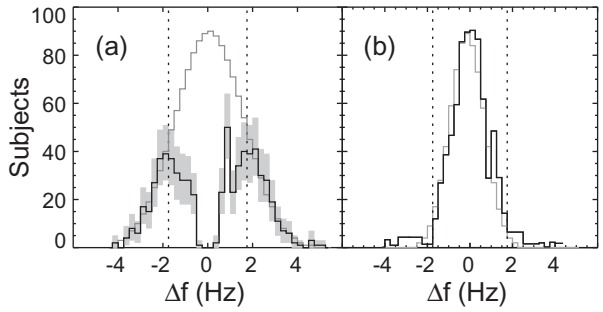

Fig. 13. Analysis of Δf ordered by laterality (Y). Shown black in (a) distribution of Δf, and (b) residue between fitted and theoretical Δf distribution. Gray plot shows in (a) the fitted Δf distribution omitting the region of ambiguity, and (b) Gaussian fitting of the residue plot. The shaded regions in (a) are the 95% confidence intervals obtained by bootstrapping with 1000 iterations. The dotted lines in both plots indicate the $|\Delta f|$ above which peaks were deemed to have good resolvability.

jects, with only 2.7% of the subjects exhibiting no discernible alpha peak as shown in Table 1. Second, the dominant alpha peak as a cluster average is located in the occipital region of the head (Figs. 9b and 10g). Third, if a fronto-central alpha peak is present it is generally weaker and has a lower frequency than that of the occipital peak. Fourth, alpha peak frequency changes with age, rising until the teenage years, then slowly declining.

(ii) Multiple alpha peaks are a common feature of spectra and need to be considered in the quantification of the alpha rhythm, with about 44% of subjects exhibiting two discernible alpha peaks. Double alpha peaks not only occur in the obvious case where there exist two clearly distinguishable peaks at a certain site, but also when distinct frequencies are spatially distinct (Chiang et al., 2008). Our automated algorithm addresses cases with multiple alpha peaks, either at single electrodes, or across sites. A difficulty encountered specific to the multiple peaks was how to distinguish the grouping of peaks. We presented a variety of ways to distinguish the two clusters but no uniquely superior solution presented itself. Hence, ordering of the two-cluster cases by their relative occipitality was employed.

(iii) We observed relationships between the alpha frequency f with the position X of the peak, with lower frequency associated with lower X (i.e., more frontal). Alpha peaks were found to shift to more frontal positions with age. This frontal shifting of the alpha peak could indicate two things: increasing power from frontal sites, or decreasing power from occipital sites. The decrease of average power P with age indicates the latter is the more probable conclusion. In Fig. 11a and b both the one-cluster and occipital cluster median fitted frequencies increase until adulthood then slowly decline towards old age, with the occipital cluster trend much weaker and not statistically significant. The frontal cluster frequency (Fig. 11c) increases with age by comparison, suggesting a dominance of the occipital cluster. In contrast Fig. 10b and c show that both of the two-cluster frequencies (frontal and occipital) increase with age, but the one-cluster frequency (Fig. 10a) increases until adulthood then slowly declines towards old age: this suggests that the relative weights of the frontal and occipital clusters shift from the higher frequency components to the lower frequency components to reproduce the age trend in the one-cluster case. Both these cases are consistent with the possibility that one-cluster cases are the result of unresolved two-cluster cases. For the double cluster cases there are greater changes in the frequency, between the old and the young, at the occipital peak than at the frontal peak.

(iv) Alpha cluster parameters change with age, often with different slopes before and after adolescence. We examined age trends of alpha parameters, extracted frequency $\langle f \rangle$, occipitality $\langle X \rangle$, laterality $\langle Y \rangle$, spatial extent $\langle s \rangle$, and averaged power $\langle P \rangle$, and found that most of these parameters varied significantly with age. The frequency and power variations with age are consistent with documented results (Niedermeyer and Lopes da Silva, 2004). In addition we found a slight dominance of the right hemisphere for all the alpha clusters (single cluster, frontal and occipital cluster in the two-cluster cases). A breakpoint age was established where the trends in the alpha frequency and the cluster position versus age change, with a typical value from 10 to 20 years of age.

(v) Fig. 11a shows males having higher peak frequencies prior to age ≈16 years in one-cluster cases, which is consistent with findings in van Albada et al. (2010) where females had a lower alpha frequency on average. Power trends also differ between males and females: Fig. 11j shows a larger decrease in males compared with females until age 20 and a small increase until the end of the age range, whereas the females have a smaller and consistent decrease in power throughout with respect to age. A similar trend can also been seen in Fig. 11l with males having a larger decrease in power compared with females.

(vi) The one-cluster case almost always lies between that of the upper and lower two-cluster cases in Fig. 10 (except in the spatial extent of the single cluster case, where the presence of the cluster is visible on almost all the electrodes examined). Fig. 10 indicate that frontal and occipital clusters evolve in parallel, so they provide no evidence for separate frontal and occipital alpha generators, a mechanism sometimes postulated for alpha generation. Whilst separate frontal and occipital generators are not totally ruled out, they would have to be affected by aging processes in the same way to account for the observations, which is unlikely. The stronger decrease in the power of the occipital cluster in two-cluster case with age, together with the trend of increased frontality both provide evidence for the hypothesis of one-cluster being a combination of two-clusters. Indeed, detailed analysis of the frequency difference Δf between the clusters in the two-cluster case shows that the one-cluster cases are consistent with being double peaks that cannot be resolved. Age trends for the one-cluster case and the higher cluster in the two-cluster cases are similar, also consistent with the hypothesis that the one-cluster case is the result of two sources that cannot be resolved. This result is consistent with previous work by Wang et al. (1992).

Several overall conclusions can be drawn from this paper. First, the automated algorithm is valuable in processing large group of subjects, and produces an easily interpreted parametrization of alpha distribution on the scalp. Second, electrode choice in single electrode studies needs to consider the variations in alpha rhythm frequency with both the electrode position and age. Most importantly, consideration of multiple peaks in the alpha rhythm is essential, given that multiple peaks had been observed in almost half the subjects.

This paper suggests several avenues to pursue in future research: (a) extension of the algorithm on a larger set of electrodes would yield higher quality cluster data for individual subjects. (b) The spatial aspects of the alpha peak are only examined briefly in this paper; a more thorough analysis between electrodes would enable detailed analysis of variations across the scalp. (c) The present method could complement low resolution brain electromagnetic tomography (LORETA) by functioning as a peak identification and quantification preprocessing stage. (d) Likewise, this method can inform time-domain analyzes (decomposition, analysis of phase and non-stationarity) by flagging the occurrence of split alpha peaks. (e) Since several common disorders show alterations of alpha activity, including ADHD (alpha asymmetry) and Alzheimer's disease (alpha slowing), a comparison of alpha peak parameters in healthy subjects versus these patient groups is likely to yield clinically important results.

Acknowledgements

This work was supported by the Australian Research Council. We acknowledge the support of the Brain Resource International Database (under the auspices of Brain Resource; www.brainresource.com) for data acquisition and processing. All scientific decisions are made independently of any BR commercial decisions via the independently operated scientific division, BRAINnet (www.brainnet.net). We thank the individuals who gave their time to take part in the study.

References

Aurlien H, Gjerde IO, Aarseth JH, Elden G, Karlsen B, Skeidsvoll H, et al. EEG background activity described by a large computerized database. Clin Neurophysiol 2004;115(3):665–73.

Bengston VL, Schaie KW, editors. Handbook of theories of aging. New York: Springer Publishing Company, Inc.; 1999.

Benninger C, Matthis P, Scheffner D. EEG development of healthy boys and girls. Results of a longitudinal study. Electroencephalogr Clin Neurophysiol 1984;57(1):1–12.

Binnie CD, editor. Clinical neurophysiology: EEG, paediatric neurophysiology, special techniques and applications. Elsevier Health Sciences; 2003.

Chiang AKI, Rennie CJ, Robinson PA, Roberts JA, Rigozzi MK, Whitehouse RW, et al. Automated characterization of multiple alpha peaks in multi-site electroencephalograms. J Neurosci Meth 2008;168(2):396–411.

Clark CR, Veltmeyer MD, Hamilton RJ, Simms E, Paul R, Hermens D, et al. Spontaneous alpha peak frequency predicts working memory performance across the age span. Int J Psychophysiol 2004;53(1):1–9.

Cohn NB, Kircher J, Emmerson RY, Dustman RE. Pattern reversal evoked potentials: age, sex and hemispheric asymmetry. Electroencephalogr Clin Neurophysiol 1985;62(6):399–405.

Díaz de León AE, Harmony T, Marosi E, Becker J, Alvarez A. Effect of different factors on EEG spectral parameters. Int J Neurosci 1988;43:123–31.

Duffy FH, Albert MS, McAnulty G, Garvey AJ. Age-related differences in brain electrical activity of healthy subjects. Ann Neurol 1984;16(4):430–8.

Dustman RE, Shearer DE, Emmerson RY. Life-span changes in EEG spectral amplitude, amplitude variability and mean frequency. Clin Neurophysiol 1999;110(8):1399–409.

Gordon E, Cooper N, Rennie C, Hermens D, Williams LM. Integrative neuroscience: the role of a standardized databse. Clin Eng Neurosci 2005;36(2):64–75.

Gratton G, Coles MG, Donchin E. A new method for off-line removal of ocular artifact. Electroencephalogr Clin Neurophysiol 1983;55(4):468–84.

Harmony T, Marosi E, de León AE Díaz, Becker J, Fernández T. Effect of sex, psychosocial disadvantages and biological risk factors on EEG maturation. Electroencephalogr Clin Neurophysiol 1990;75(6):482–91.

Inouye T, Shinosaki K, Yagasaki A, Shimizu A. Spatial distribution of generators of alpha activity. Electroencephalogr Clin Neurophysiol 1986;63(4):353–60.

Jensen O, Tesche CD. Frontal theta activity in humans increases with memory load in a working memory task. Eur J Neurosci 2002;15:1395–9.

Kaplan Alexander Ya, Fingelkurts Andrew A, Fingelkurts Alexander A, Borisov Sergei V, Darkhovsky Boris S. Nonstationary nature of the brain activity as revealed by EEG/MEG: methodological, practical and conceptual challenges. Signal Process 2005;85(11):2190–212.

Klimesch W. EEG alpha and theta oscillations reflect cognitive and memory performance: a review and analysis. Brain Res Rev 1999;29(2–3):169–95.

Marshall PJ, Bar-Haim Y, Fox NA. Development of the EEG from 5 months to 4 years of age. Clin Neurophysiol 2002;113(8):1199–208.

Matthis P, Scheffner D, Benninger Chr, Lipinski Chr, Stolzis L. Changes in the background activity of the electroencephalogram according to age. Electroencephalogr Clin Neurophysiol 1980;49(5–6):626–35.

Nelder JA, Mead R. A simplex method for function minimization. Comp J 1965;7(4):308–13.

Niedermeyer E. Alpha rhythms as physiological and abnormal phenomena. Int J Psychophysiol 1997;26(1–3):31–49.

Niedermeyer E, Lopes da Silva FH. Electroencephalography: basic principles, clinical applications, and related fields. Lippincott Williams & Wilkins; 2004.

Nunez PL, Srinivasan R. Electric fields of the brain: the neurophysics of EEG. Oxford University Press; 2006.

Nunez Paul L, Reid Larry, Bickford Reginald G. The relationship of head size to alpha frequency with implications to a brain wave model. Electroencephalogr Clin Neurophysiol 1978;44(3):344–52.

Petersén I, Eeg-Olofsson O. The development of the electroencephalogram in normal children from the age of 1–15 years non-paroxysmal activity. Neuropadiatrie 1971;2(3):247–304.

Robinson PA, Whitehouse RW, Rennie CJ. Nonuniform corticothalamic continuum model of electroencephalographic spectra with application to split-alpha peaks. Phys Rev E Aug 2003;68(2):021922.

Rubin Morton A. The distribution of the alpha rhythm over the cerebral cortex of normal man. J Neurophysiol 1938;1(4):313–23.

Samson-Dollfus D, Delapierre G, Do Marcolino C, Blondeau C. Normal and pathological changes in alpha rhythms. Int J Psychophysiol 1997;26(1–3):395–409.

Scott DF, Heathfield KWG, Toone B, Margerison JH. The EEG in Huntington's chorea: a clinical and neuropathological study. J Neurol Neurosur Ps 1972;35(1):97–102.

Shaw JC. The Brain's alpha rhythms and the mind. Elsevier; 2003.

Tarvainen MP, Hiltunen JK, Ranta-aho PO, Karjalainen PA. Estimation of nonstationary EEG with kalman smoother approach: an application to event-related synchronization. IEEE T Bio-Med Eng 2004;51(3):516–24.

Valdés-Hernández PA, Ojeda-González A, Martnez-Montes E, Lage-Castellanos A, Virués-Alba T, Valdés-Urrutia L, et al. White matter architecture rather than cortical surface area correlates with the EEG alpha rhythm. Neuroimage 2010;49(3):2328–39.

van Albada SJ, Kerr CC, Chiang AKI, Rennie CJ, Robinson PA. Neurophysiological changes with age probed by inverse modeling of EEG spectra. Clin Neurophysiol 2010;121(1):21–38.

Wang G, Takigawa M, Matsushita T. Correlation of alpha activity between the frontal and occipital cortex. Jpn J Physiol 1992;42(1):1–13.